Phase–Space Characteristics of the Tropical Stratospheric Quasi-Biennial Oscillation

RISHENG WANG AND KLAUS FRAEDRICH

Meteorologisches Institut, Universität Hamburg, Hamburg, Germany

STEVEN PAWSON

Institut für Meteorologie, Freie Universität Berlin, Berlin, Germany

(Manuscript received 8 July 1994, in final form 18 May 1995)

ABSTRACT

Extended empirical orthogonal functions (EOFs) are used to define a phase space for the analysis of tropical stratospheric wind data, extending our previous study of the quasi-biennial oscillation (QBO) in several manners. First, the sensitivity of the analysis to the length of the window (w) is discussed in some detail. As w increases, the leading pair of EOFs become more concentrated on the period near 28 months; simultaneously, the signals contained in higher-order EOFs become more significant, with more clearly defined periodicities; however, for large w more EOFs are required to represent the same variance. There appear to be two stable regimes: when w is less than 20 months the first two EOFs describe a QBO with some irregularities in the onset of easterly wind regimes, whereas when w exceeds 30 months such irregularities are represented by the third and fourth EOFs. Second, the first pair of EOFs with $w = 40$ are regarded as representing a pure QBO signal, subject to variations in cycle length (ranging from 22 to 33 months) and amplitude but propagating smoothly. Its phase–space characteristics are examined in some detail; this oscillation is regarded as a limit cycle, subject to low-frequency variability, presumably due to fluctuations in the forcing mechanisms at work. No annual cycle is evident in its propagation in phase space. Third, departures from this pure QBO are examined. These are represented by higher-order signals with $w = 40$. EOFs 3 and 4 describe much of the irregularity in downward propagation of the wind regimes, with dominant periods in a broad band centered on 28 months; EOF 5 does not represent a propagating signal but some low-frequency variability (probably externally forced) in the vertical wind shear; EOFs 6 and 7 are the subharmonics of the QBO; EOFs 8 and 9 represent the annual cycle.

1. Introduction

The quasi-biennial oscillation (QBO) of the zonal wind in the tropical stratosphere is one of the most intriguing near-periodic motions in the atmosphere. There are two quite fascinating aspects to the oscillation. The first is its near-periodicity. The second is the pronounced delay that often occurs in the downward propagation of the easterly shear zone, thus destroying the periodicity. In this study, a statistical analysis of the QBO using extended empirical orthogonal function (EOF) analysis, begun in Fraedrich et al. (1993), is continued.

Periodic vacillations of the zonal-mean wind resembling the QBO can be described by the Holton and Lindzen (1972) model (HL model). The period and amplitude of the modeled oscillation are sensitive to the strength of the tropical waves propagating into the stratosphere and the dissipation coefficients (see Holton and Linzen 1972; Plumb 1977; Hamilton 1981; Yoden and Holton 1988). The successive, downward propagating easterly and westerly wind regimes descend at a rate of about 1 km mo^{-1} (e.g., Wallace 1973), but the westerly wind onset is generally fastest. This was explained in terms of the role of the QBO-induced mean meridional circulation by Plumb and Bell (1982).

Such models, subject to steady lower-boundary forcing, generate repeating oscillations. In the real atmosphere this may not be the case: tropical waves are observed sporadically and are believed to be associated with large-scale convective activity. A body of work has concentrated on the response to long-term variations in the tropical wave forcing. Two of the most obvious features of the atmospheric circulation are the El-Niño/Southern Oscillation (ENSO) in the tropical ocean–atmosphere system and the annual cycle.

ENSO events affect the convective systems that determine the generation of tropical waves. Maruyama and Tsuneoka (1988) discussed a possible relationship between warm ENSO events and the descent rate of the westerly shear zones. Isolation of an ENSO signal in the QBO has generally proven difficult; Xu (1992) concluded that there was no relationship between the two phenomena on the basis of a statistical analysis using principal oscillation patterns.

Corresponding author address: Dr. S. Pawson, Institut für Meteorologie, Carl-Heinrich-Becker Weg 6–10, 12165 Berlin, Germany.
E-mail: pawson@strat01.met.fu-berlin.de

Maruyama (1991) presented evidence of an annual cycle in the amplitude of observed mixed Rossby–gravity wave. The effect of this was investigated by Dunkerton (1990), who suggested that it modulates the onset of easterly winds at 50 hPa, which is often delayed during Northern Hemisphere winter. Dunkerton proposed that this modulation causes much of the internal variability of the QBO. Dunkerton (1991) argued further that the remotely driven Brewer–Dobson upwelling reduces the descent rates of the shear zones; in particular, he showed that the tropical wave fluxes must be increased considerably to retain the period of the QBO against the vertical advection of winds.

Lindzen and Tsay (1975) had already suggested that the tropical mixed Rossby–gravity waves in the atmosphere are too weak to provide the necessary momentum for the easterly phase of the QBO. Takahasi and Holton (1991) showed that a planetary-scale, westward propagating gravity wave, too shallow to isolate in radiosonde data, could also provide the necessary momentum for this phase of the QBO. The role of smaller-scale gravity waves, which would act locally, has not yet been investigated. It is assumed that the mechanism of the HL model drives the QBO, even if the details of the waves are different. Hirota and Sato (1969) suggested that extratropical planetary waves could propagate into the tropical stratosphere, where their dissipation could provide an additional easterly body force.

Using wind data from the Tropics and midlatitudes, Pawson et al. (1993a) speculated that the descent of the easterly wind regime is reversed in northern winter but that this is offset by additional easterly forcing close to the zero wind line, presumably due to the dissipation of equatorially propagating Rossby waves from the Northern Hemisphere. This is an inherently nonlinear relationship with very low linear correlation coefficients because it depends on the phase of the QBO itself.

This paper presents a study of the variability of the QBO using a phase–space approach. This was introduced by Wallace et al. (1993), who showed that EOF decomposition of the tropical wind data leads to two dominant EOFs that describe the QBO. The angular speed of progression of the orbits in phase space are related to the downward propagation of the wind regimes; the annual cycle in this phase progression was evident. Fraedrich et al. (1993) used extended EOFs to analyze the same time series. Such analysis provides a straightforward way of characterizing the QBO signal in phase space with direct relationship to the space–time structure in physical space. Here the study of Fraedrich et al. (1993) is extended using data described in section 2. More attention is devoted to the choice of window in the extended EOF analysis (section 3). The dynamics of the "pure" QBO are examined in section 4: in particular, characteristics of the low-frequency variability of the QBO are discussed. Higher-order signals, representing departures from the pure QBO, are discussed in section 5: links with the annual cycle and ENSO are sought. The discussion and conclusions are in section 6.

2. The wind data

As in Fraedrich et al. (1993) monthly mean tropical zonal wind data at seven levels (70, 50, 40, 30, 20, 15, and 10 hPa), updated from Naujokat (1986) in Pawson et al. (1993b), are used. The time series includes 480 months (40 years) from January 1953 until December 1992.

The 10-hPa data from the first three years are missing. They were linearly interpolated using a multiple regression technique with the data at 70 and 15 hPa. Tests showed that the effect of errors in the regression are negligible, which was expected since the correlation is highly significant and the missing part of the time series is relatively short.

3. Extended EOF analysis: Sensitivity to choice of window

To study the underlying variability of the QBO from observed signals, it is necessary to establish a coordinate system to describe the state of the system and its time evolution. In terms of dynamical system theory, this is referred to as the phase–space reconstruction. The phase space is defined as an arbitrary set of coordinates that uniquely define the state of the system at time t along a trajectory that describes the smooth change of the system in physical space. Typically, the trajectory settles on a compact subset of the phase space (the attractor). The phase–space reconstruction involves representing this attractor sufficiently with a small number of variables. One commonly used method of reducing the number of variables is to use the leading EOFs as the basis of the phase space containing the attractor. The projection of the attractor onto the EOFs leads to a set of new variables referred to as principal components (PCs). This approach facilitates a geometrical description of the dynamics of the underlying system. The variability is then characterized by topological features in phase space. For physical interpretation we rely on the study of the EOF patterns and the PCs.

a. Extended EOF analysis

Traditional EOF analysis utilizes a time series of data and examines the temporal behavior of spatial patterns. The extended EOF analysis (Weare and Nasstrom 1982) recognizes that the temporal evolution of the spatial patterns is also an important part of the evolution and introduces a sliding window of length w into the EOF analysis (Fig. 4 of Fraedrich et al. 1993). A more detailed discussion of extended EOFs is given by Wang (1994). Studies of the QBO using EOF analysis

were presented by Wallace et al. (1993) for the traditional case (w = 1 mo) and for extended EOFs (w = 15 mo) by Fraedrich et al. (1993).

In this study the notation EOF_i^w is used to represent the ith eigenvector with window w; its principal component (amplitude) is represented by PC_i^w.

In Fraedrich et al. (1993) the extended EOF analysis was performed using a window of length w = 15 mo, although some results using w = 40 mo were also discussed. The results of that study showed how the choice of longer windows led to much smoother reconstructed time series and smoother phase progression in phase space, especially compared to the choice of w = 1 mo. In particular, the first four EOFs with w = 40 were required to represent the same features as the first two EOFs with w = 15. In the remainder of this section more detailed attention is given to the sensitivity of the results to the choice of w.

b. Periodicities

In Fraedrich et al. (1993) we proposed that the use of extended EOFs facilitates the separation of physically meaningful signals within the data. Further evidence in support of this idea is given here. Spectral analyses of the leading ten PCs of the EOF analyses using two windows, w = 1 and w = 40 is shown in Fig. 1. Along with the power spectra of the PCs, the 95% significant departures from red-noise signals are included. These were determined from the red-noise spectrum, $R(\nu)$, as a function of frequency (ν), calculated as a first-order Markov process (Box and Jenkins 1976):

$$R(\nu) = P\left[\frac{1-\alpha^2}{1-2\alpha\cos\left(\frac{2\pi\nu}{n}\right)+\alpha^2}\right], \quad (1)$$

where P is the mean power and α is the autocorrelation coefficient at 1-month time lag. The significance levels were then determined by assuming a χ^2 distribution. The analysis with w = 1 (as in Wallace et al. 1993) shows that only the leading pair of EOFs have significant power at the 28-month period; EOF_3^1 and EOF_4^1 just exceed the 95% significance levels over a wide range of periods ranging from 6 to 12 months, while EOF_5^1 to EOF_7^1 are not distinguishable from red-noise signals. In contrast, EOF_1^{40} to EOF_{10}^{40} each has a significant signal. The two leading PCs have power on the 28-month timescale; the next pair have broad peaks that exceed the 95% significance level for periods between 12 and 50 months; EOF_5^{40} has a peak close to 12 months and some lower-frequency variability that does not quite attain 95% significance; the next two pairs have identifiable peaks at 14 months (the subharmonics of the QBO) and the annual cycle.

A more detailed picture of the sensitivity of the periodicities to the choice of w is given by plots of the power of PC_1^w, PC_3^w, and PC_5^w against increasing w from 1 to 40 months (Fig. 2). As w increases, the spectrum of the PC_1^w becomes more sharply defined, with shorter-scale fluctuations for w < 17 month at periods that become insignificant for larger w. Although the power of PC_1^w increases only slowly for w > 20 months, this is not true of the higher-order signals. The maximum power of PC_3^w slowly increases from the barely significant values of less than one year for small w up to the 28-month period of the QBO by w = 40. The width of the period range exceeding 95% significance is considerably broader than that for PC_1^w. The dominant power of PC_5^w also increases with increasing w but always remains at shorter periods than the QBO itself, except that at large w the second, long-period maximum appears, with a region of very low significance centered on 28 months.

In summary, as w increases, the extended EOF analysis selectively narrows the period band contained in the first two EOFs, their signal becoming more concentrated on 28 months for larger windows.

c. Phase progression

Wallace et al. (1993) associated the propagation of the QBO in physical space with the phase progression in the space spanned by the two leading PCs with w = 1. The increased smoothness of the orbits in the PC_1^w-PC_2^w plane as w increases was noted in Fraedrich et al. (1993). In this phase space, both the phase speed (rate of angular progression) and the amplitude modulation (the displacement from the center) can both be determined. These were calculated as follows. Following Wallace et al. (1993) the trajectory in polar coordinates ($A(t)$, $\phi(t)$) is defined by the amplitude $A(t)$ at time t as the distance

$$A(t) = [PC_1^w(t)^2 + PC_2^w(t)^2]^{1/2}$$

and the corresponding phase speed $\phi(t)$ as the angular progression of the orbit per month

$$\phi(t) = \Phi(t+1) - \Phi(t),$$

where

$$\Phi(t) = \arctan\left[\frac{PC_2^w(t)}{PC_1^w(t)}\right]$$

is the phase angle in month t.

The phase speeds of the trajectories in the PC_1^w-PC_2^w plane with w = 1, 8, 15, 30, and 40 mo (Fig. 3) show that those for w = 30 and 40 mo have very similar low-frequency fluctuations, whereas ϕ displays abrupt and large changes for shorter w. This is particularly pronounced for w = 1 since no smoothing has been performed [Wallace et al. (1993) applied a 5-month running mean to the wind data]. This occurs because the high-frequency variations found with short windows (w < 15 mo) in Fig. 3 are represented in the

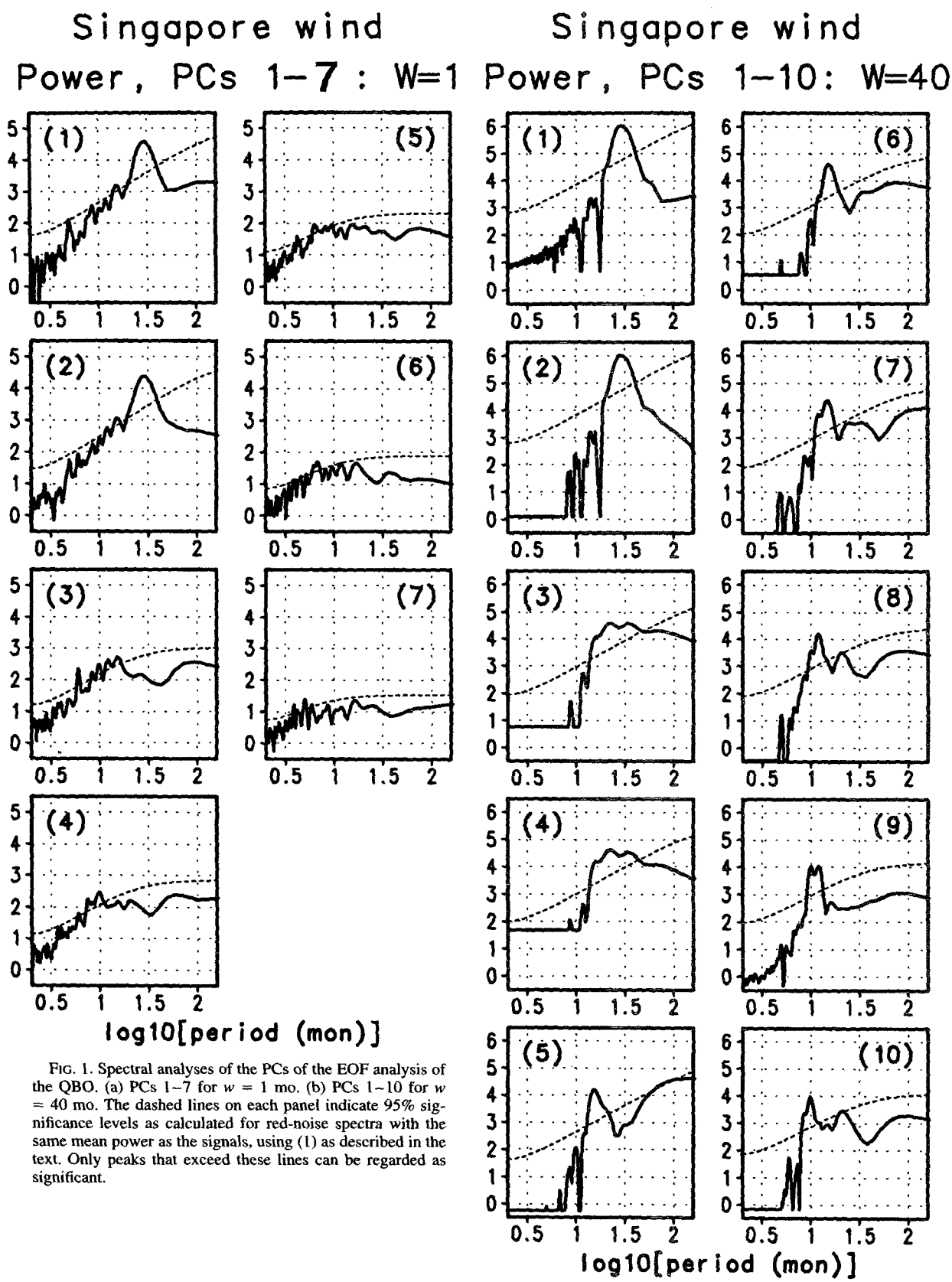

FIG. 1. Spectral analyses of the PCs of the EOF analysis of the QBO. (a) PCs 1–7 for w = 1 mo. (b) PCs 1–10 for w = 40 mo. The dashed lines on each panel indicate 95% significance levels as calculated for red-noise spectra with the same mean power as the signals, using (1) as described in the text. Only peaks that exceed these lines can be regarded as significant.

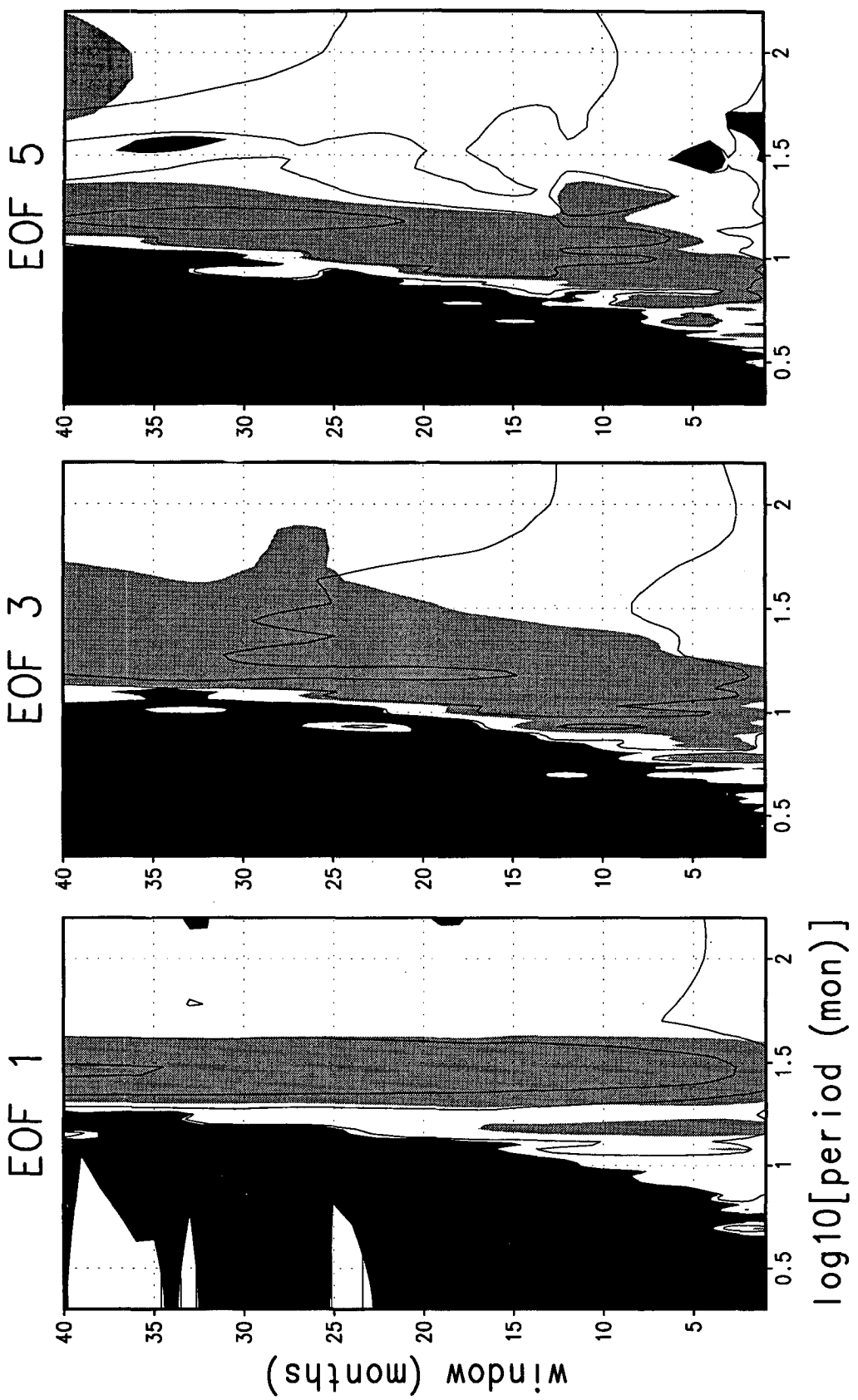

FIG. 2. Power of the spectral analyses of the PCs against w. (a) PC_1^w, (b) PC_3^w, and (c) PC_5^w. In all cases significant power (see text for details) is shaded gray, and extremely low values, where there is much noise, are shaded black.

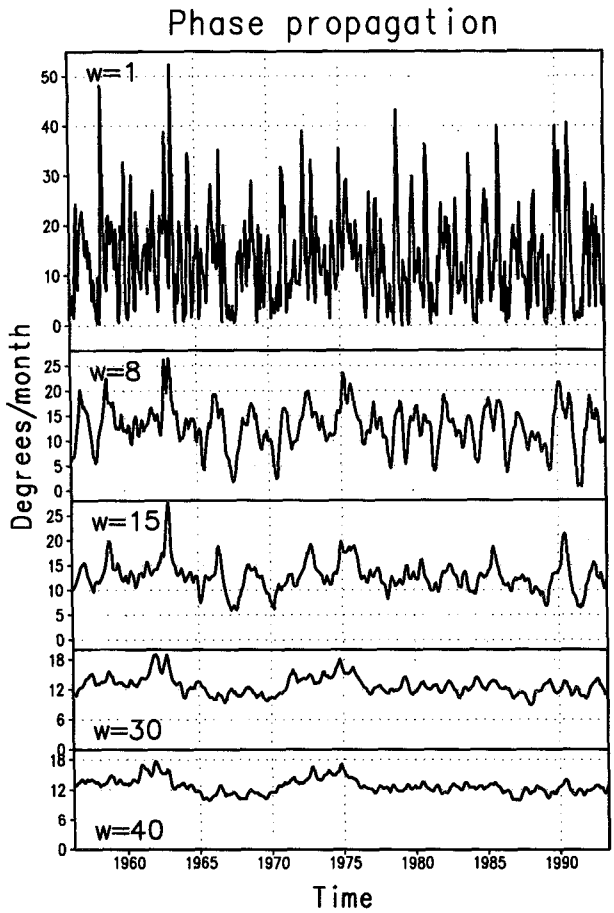

FIG. 3. The phase speed $\phi(t)$ in the (PC_1^w, PC_2^w)-plane (ordinate, degree/month) as a function of month (abscisca) derived from embedding windows of w = 1, 8, 15, 30, and 40 mo.

subspace spanned by higher-order EOFs obtained with larger windows ($w > 27$ mo). An important point concerns the annual modulation of phase speed found by Wallace et al. (1993), consistent with Dunkerton's (1990) results in physical space. In the extended EOF analysis, the signal of the annual cycle is found in higher-order patterns (e.g., EOF_8^{40} and EOF_9^{40}) and there is no annual modulation of ϕ for the oscillation described by the first two EOFs.

Similar remarks can be made about the amplitudes of the orbits in phase space (Fig. 4) that represent increasingly less high-frequency structure as w increases.

Further evidence as to the stability of the analysis for large w comes from the correlation of the first ten PCs for w = 35 with those for w = 40 (Table 1), which shows a high correlation (or anticorrelation, meaning simply that the signs of both the PC and the EOF have changed) along the diagonal and generally insignificant values elsewhere. This also illustrates the robustness of the extended EOF analysis against degeneracy and suggests that the higher-order signals (say $i > 5$) are physically meaningful.

d. EOF structures

The structure of the first five extended EOFs for w = 15 is given in Fraedrich et al. (1993). Recall that the first pair of EOFs always represent the QBO motion, although with increasing w they become smoother. The behavior of the higher-order eigenvectors is more intriguing since the dominant period increases with increasing window (Fig. 2). To illustrate these variations, the structure of EOF_3^w with changing window is shown in Fig. 5; similar behavior is shown by EOF_4^w. The tendency to represent low frequencies is represented not only in the power but also in the tendency for the pattern to include ever more slowly propagating wavelike motions. It must be stressed that for intermediate w (10–30 mo) this pattern has a structure resembling propagation in the lower stratosphere but steady motion at higher levels, with a gradual transition to a propagating signal with period 28 months for $w > 34$ months. The physical meaning is that for large windows EOF_3^w includes features of the time delay in onset of easterlies, whereas for intermediate w it represents higher-order departures since the stalling of the easterly descent is already included in the first two EOFs.

e. Discussion: Choice of window

In this section a more detailed analysis of the choice of w has been presented than in Fraedrich et al. (1993). There is a tendency for the lowest-order EOFs to become more sharply concentrated on the QBO period as

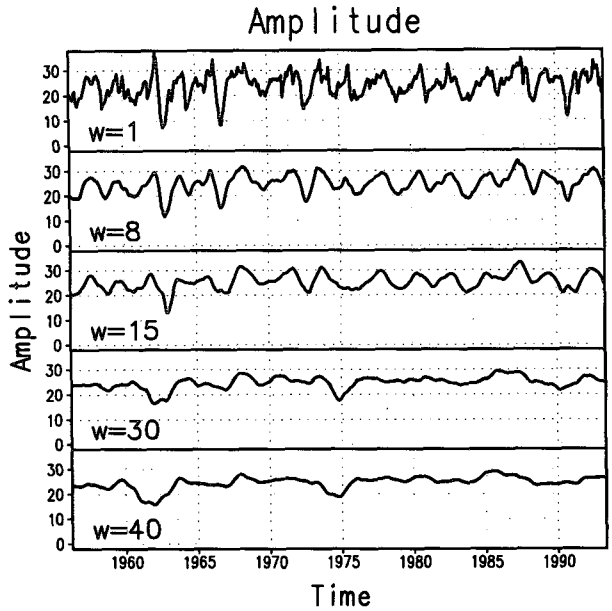

FIG. 4. The amplitudes $A(t)$ in the (PC_1^w, PC_2^w)-plane (ordinate, degree/month) as a function of month (abscisca) derived from embedding windows of w = 1, 8, 15, 30, and 40 mo.

TABLE 1. Cross correlations ($\rho \times 100$) between the first ten leading PCs derived from the time windows of $w = 35$ (row) and $w = 40$ (column).

	PC_1^{35}	PC_2^{35}	PC_3^{35}	PC_4^{35}	PC_5^{35}	PC_6^{35}	PC_7^{35}	PC_8^{35}	PC_9^{35}	PC_{10}^{35}
PC_1^{40}	97	−26	0	1	2	1	0	0	−1	0
PC_2^{40}	25	96	−2	0	−1	−3	1	−3	−1	−2
PC_3^{40}	−1	2	91	35	11	16	−3	2	−1	0
PC_4^{40}	1	−1	37	−86	−26	−1	19	−1	−6	0
PC_5^{40}	2	−1	1	33	−92	−6	14	−1	0	1
PC_6^{40}	0	4	−15	−6	−10	94	−3	19	0	2
PC_7^{40}	1	0	7	−16	−22	−7	−89	5	22	−2
PC_8^{40}	1	3	4	0	2	−23	15	76	14	20
PC_9^{40}	−2	1	−3	2	−4	−8	−25	23	−85	0
PC_{10}^{40}	0	−1	−3	−1	−1	−2	5	48	17	−51

w increases. There appear to be two quasi-stable regimes in the analysis, one for intermediate w (around one-half a period of the QBO) and one for $w > 28$ months. In the first, the propagating QBO signal, including delays in its downward propagation, is represented by the first two EOFs (Fraedrich et al. 1993); in the second, the higher smoothing in the analysis is reflected in the need to use more EOFs to represent the same variability. Since the eigenvalues of the corresponding EOFs reflect the variances of the PCs, it is not surprising that the distribution of the eigenvalues (not shown) shows qualitatively the same behavior. The patterns of the EOFs also display a similar behavior.

Exactly which window to use depends on the application. The reason for the choice of $w = 40$ in the remainder of this study is that larger windows favor the separation of different-scale dynamics and thus, hopefully, enable the identification of physically meaningful signals in the data. This is often possible owing to the scaling properties of atmospheric dynamics: large-scale (space–time) dynamics tend to contribute more to the total variance than small scales and to the fact that the characteristic oscillation (or normal modes, such as the QBO), as well as the external forcing (such as the annual modulation), often have their own particular scale range of the spectrum. The extended EOFs in the present context select space–time correlation patterns according to their variance contribution.

For $w = 40$, EOF_1^{40} to EOF_{10}^{40} describe almost 91% of the variance of the tropical wind dataset. This is equivalent to the first five extended EOFs with $w = 15$ and the first pair with $w = 1$ mo.

4. Characteristics of the QBO

a. The pure QBO signal

Hovmöller diagrams of the vertical-time structure of the tropical winds (e.g., Naujokat 1986) clearly show the downward propagation of the alternating wind regimes of the QBO. In Fraedrich et al. (1993) the reconstructed time series from various EOFs were shown (Fig. 5c of that paper). With $w = 40$ months the time series reconstructed from the first two EOFs shows a regular downward propagation but with some variations in amplitude and period; these can be related to the variations in phase speed and amplitude in physical space (Figs. 3 and 4).

The phase portrait of PC_1^{40} against PC_2^{40} shows the smooth progression of these orbits (Fig. 6), emphasising their regularity in comparison to those with $w = 1$ and $w = 15$ mo (Figs. 3 and 7 in Fraedrich et al. 1993). The structures of the first ten EOFs with $w = 40$ (Fig. 7) show that the leading two EOFs are a degenerate pair, with essentially the same structure (successive smooth downward propagation of the wind regimes), but they have a time shift of one-quarter of the average QBO cycle (orthogonality). They explain 74% of the total variance of the tropical wind data.

Although there are variabilities in the dynamics of the QBO reconstructed from these two EOFs, its general structure is very similar to the idealized QBO obtained from suitable variants of the HL model. Hence the dynamics defined in the (EOF_1^{40}, EOF_2^{40})-plane can be referred to as the pure QBO signal determined from observations.

The pure QBO signal defined here makes no assumptions about periodicity and places no restrictions on the amplitude, as would be the case in the HL model with steady lower-boundary forcing. This is a great advantage to the later analysis where deviations from the pure QBO (the higher-order patterns in Fig. 7) will be examined. It is assumed that the intrinsic dynamics of the tropical lower stratosphere are described by this pure QBO, whose precise details depend on the various forcing mechanisms acting. Delays in propagation are then represented by excursions from the (EOF_1, EOF_2)-plane (Fig. 6), represented by higher-order EOFs, which allow for crossings of the orbits in Fig.

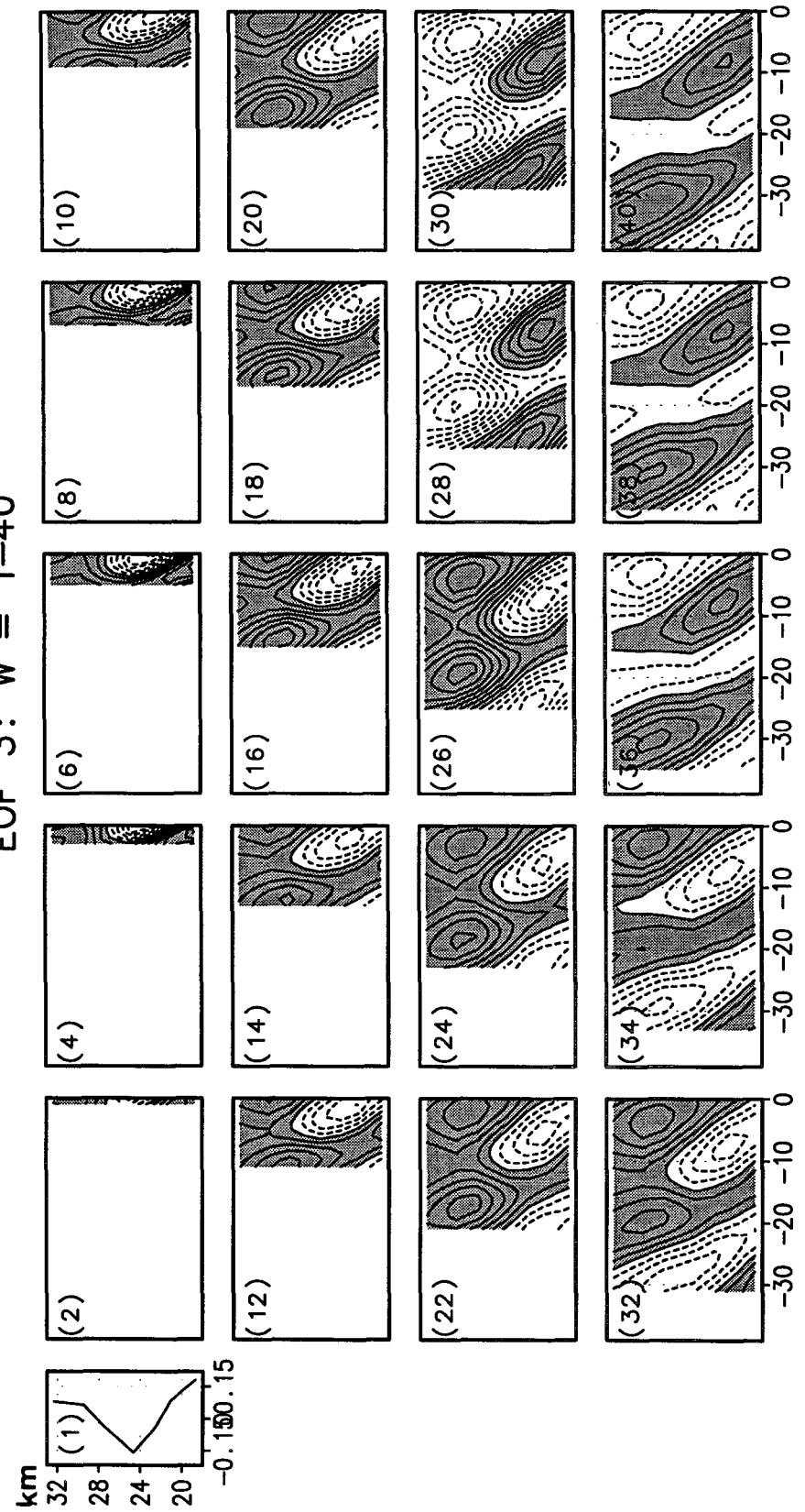

FIG. 5. The height–time delay structure of EOF_3^w as a function of w.

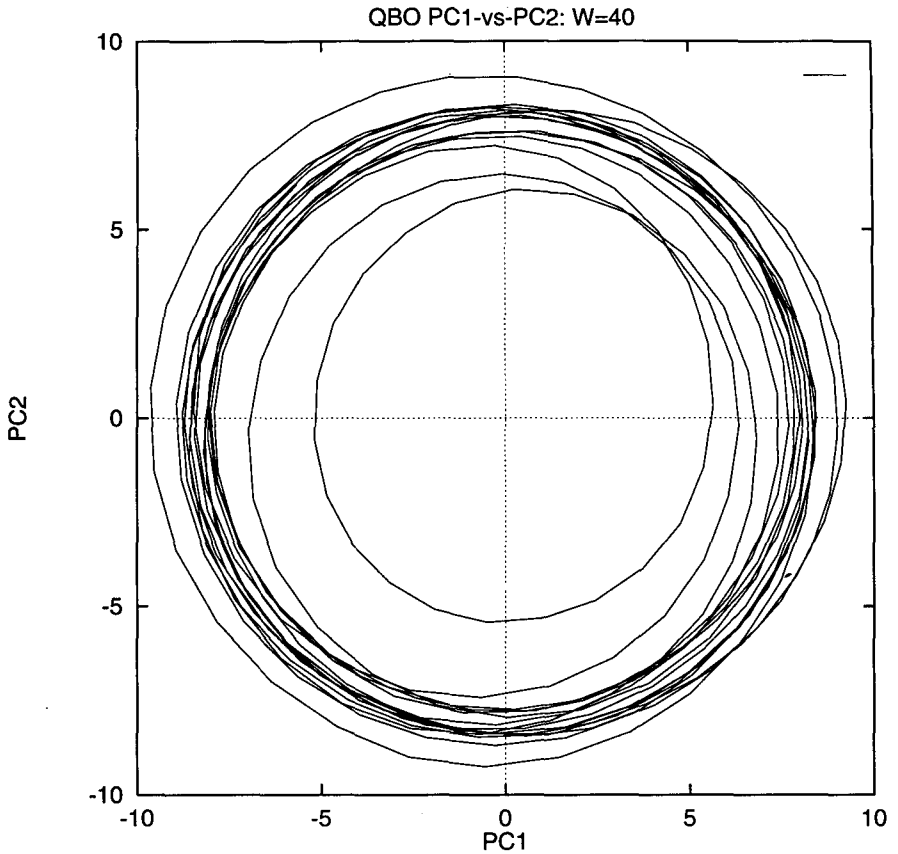

FIG. 6. The phase–space plot in the (EOF_1^{40}, EOF_2^{40})-plane.

6. These excursions describe the observed irregularities in the observed QBO, as discussed later sections.

The variability of this pure QBO signal will be examined in more detail.

b. The variability of the pure QBO signal

1) VARIABILITY OF THE ORBIT PARAMETERS

The angular propagation (Fig. 3) and the amplitude (Fig. 4) of the phase space spanned by EOF_1 and EOF_2 (Fig. 6) show low-frequency variability. In particular, the amplitude $A(t)$ changes on a decadal scale, whereas the phase propagation ϕ is more subjected to shorter variations, mostly less than 3 years. This suggests that the amplitude of the QBO is insensitive to small-scale changes, whereas the phase speed (the rate of downward propagation of the zonal wind) is more subjected to small-scale changes. On large scales, $A(t)$ and $\phi(t)$ are significantly anticorrelated, indicating that the zonal wind regimes descend faster when the amplitude is small. There are various possible reasons for this: for instance, the period and amplitude of the QBO in the HL model are sensitive to the strength of the tropical waves.

Variations in ϕ lead to changes in the duration of the wind regimes. There are 15 full cycles during the observation; their durations in the reconstruction of the pure QBO range from 22 to 33 months (Table 2). Plots of $A(t)$ and $\phi(t)$ against the calender month reveal no obvious annual or semiannual cycles. There is also no clear relationship to the Southern Oscillation index.

Thus, the reason for the observed variability in the pure QBO is not clear to us. It could be due to long-term variations in the tropical wave forcing. Other forcing mechanisms (vertical advection or planetary waves) may also play a role. Isolation of these effects would require the simultaneous investigation of the winds with these various possible forcing mechanisms, which is not possible with the data available. Another possibility is that it is an intrinsic variability arising from stochastic wave forcing. The question is whether a stochastically driven dynamical system can display a low-dimensional attractor: this is investigated next, although it is difficult to obtain a definitive answer from the short dataset available (only 15 cycles).

2) POINCARÉ SECTIONS

The geometrical structure of the pure QBO (Fig. 6) did suggest a strong restriction to the number of degrees

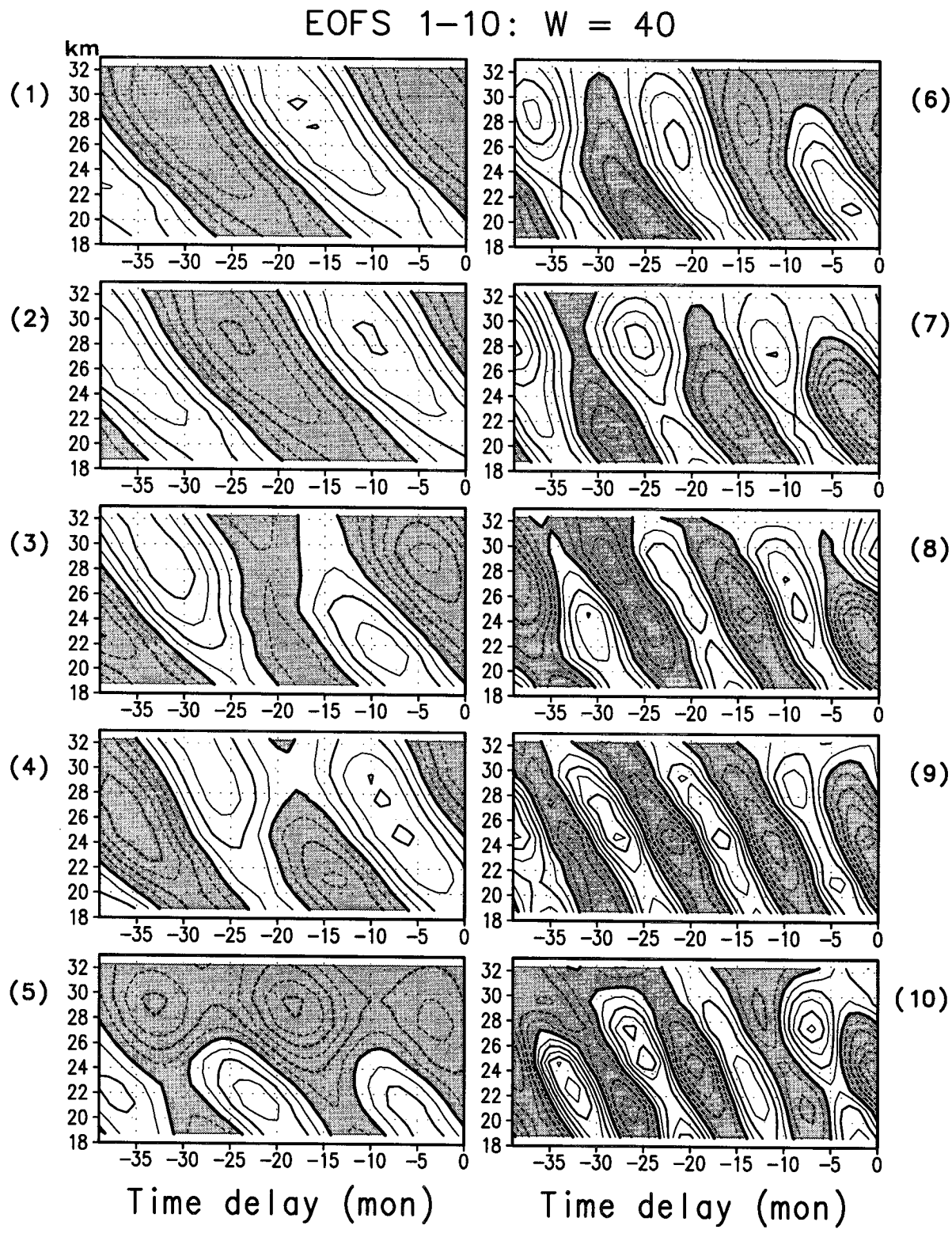

FIG. 7. The height–time delay sections of EOF_1^{40} to EOF_{10}^{40} (panels 1 to 10, respectively). Negative values are shaded and the (nondimensional) contour interval is the same on all panels.

TABLE 2. The frequency of occurrence of the different periods of the QBO reconstructed from the first two EOFs with $w = 40$.

	(mo)											
Length of period	22	23	24	25	26	27	28	29	30	31	32	33
Accumulated frequency	1	0	1	1	1	3	0	3	2	1	1	1

of freedom of the system. In order to get a feeling about whether there is a structure underlying the observed change, we first examine the Poincaré section. Suppose that the attractor can be embedded in three-dimensional Euclidean space, and by cutting the attractor with a two-dimensional plane the trajectories intersect the plane, leading to a set of points on the plane, which is called a Poincaré section (see, e.g., Schuster 1989). This is topologically equivalent to the next-maximum map (see Lorenz 1963) obtained by plotting the local maximum (of, say, PC_1) in any one cycle against its maximum in the next cycle. For deterministic processes the sections have definite structure: Figs. 8c,d show the Poincaré sections derived from linear combinations of two sine waves (periods of 12 and 11 or 5 months); the corresponding plots for variables x and z of the Lorenz attractor (Figs. 8e,f) also display a regular pattern. If there is no obvious structure of the points, there are two possible conclusions: either the observed change is due to stochastic process, or the dimension of the attractor is much higher than 3. The Poincaré maps for PC_1^{40} and PC_2^{40} (Figs. 8a,b) seem to show a geometrical structure and a certain time order. Note the appearance of the time sequence (particularly in Fig. 8b): orbits 2, 7, and 12 follow orbit 3, 8, and 13, respectively. It appears to have some deterministic order within a certain timescale range, however, some disorder also exists. Although it is not sufficient to draw a robust conclusion based on only 15 points, we feel that the dimension of the QBO is not very high: the two-dimensional plane is already a good approximation of the observed dynamics (Fig. 7). We must point out that finiteness of the dimension of a dynamical system does not necessarily mean that one can build a finite-dimensional physical model of the system. In the case of QBO, as the wave–mean flow interaction is involved with smooth downward movement of the interaction zone, a partial differential equation is needed to model the process, which means an infinite degree of freedom (which equals the number of the initial values). However, the state of the system (or the model output) can evolve on the low-dimensional attractor, which can be described in a phase space of finite dimensionality.

3) NEAR-NEIGHBOR BEHAVIORS

The near-neighbor behavior is often studied by examining how initially close trajectories diverge with the time evolution. By examining the near-neighbor behavior, one is able to show whether the underlying dynamics is linear, nonlinear, or stochastic. For linear processes, initially close points in phase space will remain close as the time evolves; for nonlinear processes they will diverge exponentially with time but undergo a continuous change within a certain time span; for stochastic process, this change can only be described in terms of probability distribution, where the changes appear mostly eratic. Usually one needs a large amount of data in order to deduce a quantitative measure (such as the Lyapunov exponents and Kolomogrov–Sinai entropy, e.g., Schuster 1989). For the limited data available for this study a more qualitative suggestion must suffice. Thus, the near-neighbor behavior will be examined by following the time evolution of the distance $[H(t)]$ of a pair of initially close points on the (EOF_1^{40}, EOF_2^{40})-plane, where

$$H(t) = [(PC_1^{40}(t + t_0) - PC_1^{40}(t + t_0 + \theta))^2 + (PC_2^{40}(t + t_0) - PC_2^{40}(t + t_0 + \theta))^2]^{1/2}$$

for $t = 0, 1, \cdots, K$, where t_0 is a arbitrarily chosen initial time such that $H(0)$ is minimum, and θ should be sufficiently large so as to ensure the initial points do not fall in the same trajectory. Figure 9a shows the time evolution of the distance $H(t)$ (ordinate in $\log_{10}$), where the abscissa is the time (month). For comparison, two pairs of points are chosen, differing by about 180° in the (EOF_1^{40}, EOF_2^{40})-plane. Note that both curves show a rapid separation at the beginning, a gradual saturation at the upper bound of the attractor, followed by a return of the states at times: a clear sign of recurrence. Note also the continuity in the change of the distances.

We have also calculated the separation of a nearby trajectory, $H(t)$, in the four-dimensional space spanned by the four leading EOFs. The result shows qualitative agreement with features obtained from Fig. 9a, that is, the exponential separation at the beginning and the recurrence (figure not shown). Meanwhile, the lagged-autocorrelation can often provide information about the dynamical behavior (memory about the initial condition) in an ensemble statistical sense:

$$\rho(\tau) = \frac{\text{cov}(\tau)}{\text{cov}(0)} \quad \text{for} \quad \tau = 0, 1, 2, \cdots, M,$$

where $\text{cov}(\tau) = 1/(n - \tau + 1) \sum_{k=1}^{n-\tau+1} (u(k) - \bar{u}) \cdot (u(k + \tau) - \bar{u})$ is the autocovariance at the time-lag

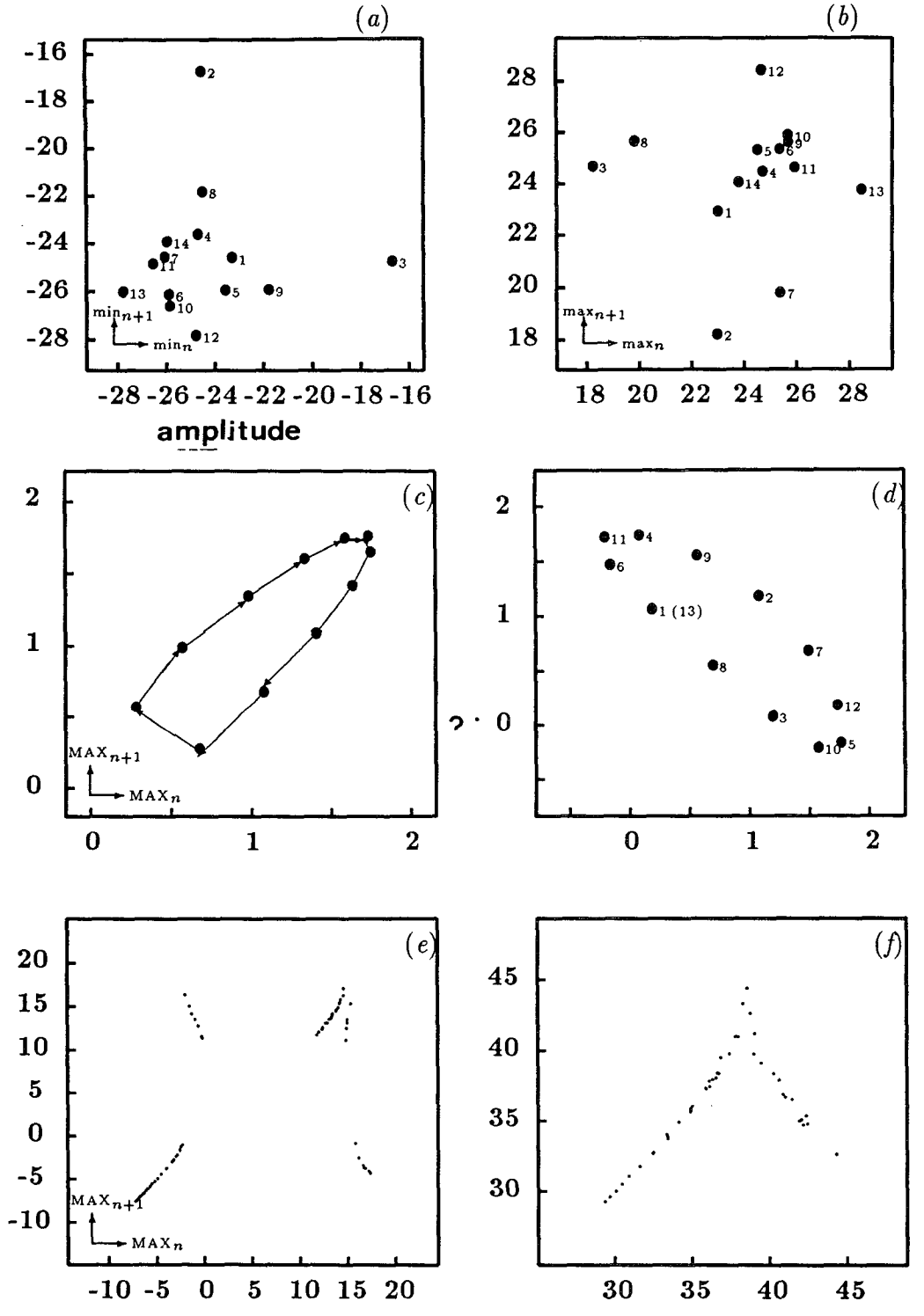

FIG. 8. Next-maximum maps (topologically equivalent to Poincaré section), constructed by plotting a local maximum of a time series against the next maximum of the same time series. (a) For PC_1^{40}, (b) for PC_2^{40}. (c) For linear combinations of two sine waves with periods of 12 and 11 months; (d) as in (c) but for periods of 12 and 5 months. (e), (f) For the variables x and z of the Lorenz (1963) model, which is embedded in three-dimensional space and displays a chaotic attractor with dimension close to 2.

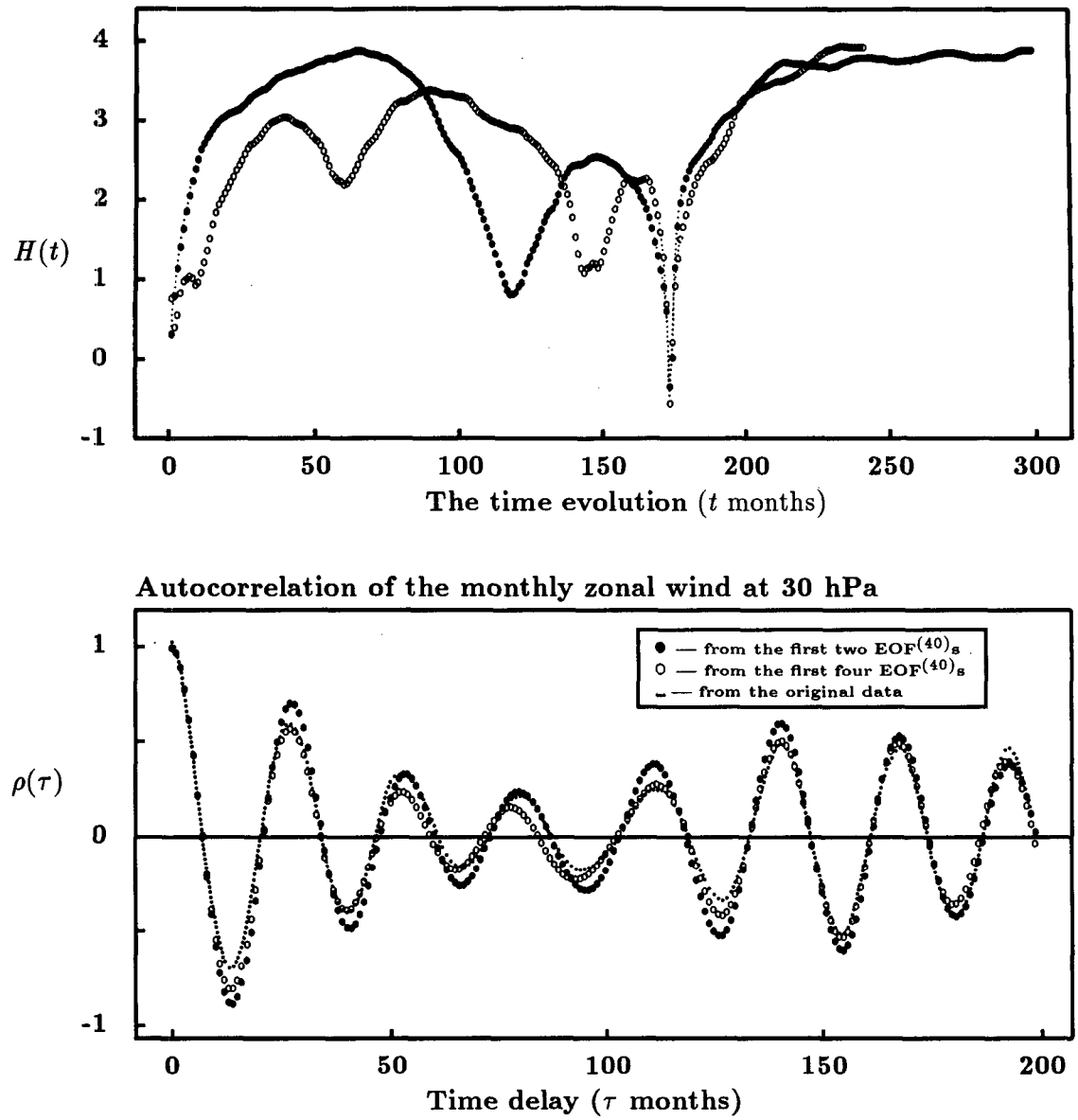

FIG. 9. The changes in distance $H(t)$ (ordinate, in $\log_{10}$) between (a) two initially close points on the (EOF_1^{40}, EOF_2^{40})-plane and (b) the lagged-autocorrelation $\rho(\tau)$ (ordinate) derived from the 30-hPa zonal wind data. In both panels, the abscissa is the time (month), representing volution time t and the time lag τ, respectively.

of τ months. Figure 9b shows the autocorrelation function $\rho(\tau)$ (ordinate) of the monthly mean zonal wind at 30 hPa displayed as a function of the time-lag τ months (abscissa). The three curves are derived from the reconstructed Hovmöller diagrams based on the first two EOFs (i.e., the pure QBO signal), the first four leading EOFs, and the original data. In all three cases, $\rho(\tau)$ displays a rather regular fluctuation, as is expected from the QBO. However, the amplitude of $\rho(\tau)$ changes from the maximum of 1.0 at $\tau = 0$ to a minimum of about 0.4 after two cycles and reaches a second maximum of about 0.7 after four cycles. This shows that such a regular structure (with a certain memory of the initial condition) cannot be produced by a purely stochastic system.

4) SUMMARY: THE CHARACTER OF THE PURE QBO

From the near-neighbor behavior (Fig. 9a) and the Poincaré section (Fig. 8) it can be deduced that the underlying dynamics are neither a pure linear wave motion nor a purely stochastic process. One likely explanation is that the QBO is a quasi-linear wave with stochastic forcing superimposed, leading to departures

from the underlying wave motion. On the other hand, there seem to exist some deterministic elements within certain timescales in the underlying dynamics that work like an inertia to smooth out the stochastic forcing.

5. Asymmetry of the QBO

Since EOF_1^{40} and EOF_2^{40} are considered as being characteristic of the pure QBO signal, the study of its asymmetric features is reduced to the examination of the higher-order EOFs and the subspaces they span. The three-dimensional structure of the phase–space propagation of the QBO is shown by Fig. 10: the EOF_1–EOF_2 plane is extended by the vertical dimensions represented by EOF_3^{40} to EOF_{10}^{40}. These phase portraits show the relationship of the propagation in the EOF_1^{40}–EOF_2^{40} plane to excursions into the higher-order signals. Note that the EOFs are orthogonal, which means that they are unrelated in the linear sense. For dynamical systems, they are often related in a nonlinear way by the mutual cross-correlations at certain timelags, as displayed in Table 3, and by the smooth orbits of the 3D phase portraits (Fig. 10).

a. Delays in onset: EOF_3^{40} and EOF_4^{40}

This pair of EOFs have their dominant power on the QBO timescale (Fig. 1), indicating that they are dependent on the phase of the QBO. Indeed, as discussed in Fraedrich et al. (1993), these patterns act to introduce the asymmetry in the QBO time series. Their structures (Figs. 7c,d) are in phase with those of the first two EOFs for about one-half of the time window but out of phase for the other half. This means that when their amplitudes are in phase with those of the first pair, they act to reinforce the first pair in the latter half of the window but to weaken it in the first half (and vice versa). In Fraedrich et al. (1993) it was noted that no equivalent pair of EOFs appear with $w = 15$ since the shorter window does not require this modification. In fact, the use of $w = 40$ leads to the existence of the patterns representing the delay in onset of the easterly phase of the QBO, whereas with $w = 15$ the delay in onset is represented by a change in the angular propagation of the first two EOFs.

In Table 3 the maximum correlations and anticorrelations between the EOFs are shown, along with the time-delays of these maxima. As a reference, the relations between PC_1^{40} and PC_2^{40} show the propagation of the pure QBO signal, with the strongest negative cross correlation (99%) occurring at ±7 months delay (one-quarter of a period) and autocorrelations (94%) occurring at 14 months. In contrast, the values for PC_3^{40} and PC_4^{40} show that the wave does not propagate for an entire period, with maximum negative cross correlations of 85% after ±6 months but autocorrelation minima of 43% at 12-months lead for PC_3^{40} and 53% at 11-months lag for PC_4^{40}.

There are thus only very weak linear correlations between the pairs (PC_1^{40}, PC_2^{40}) and (PC_3^{40}, PC_4^{40}). However, inspection of the time series of the PCs reveals clearly that the dominant extrema in (PC_3^{40}, PC_4^{40}) occur at the times when (PC_1^{40}, PC_2^{40}) have their minimum amplitudes. The relationship between these two pairs of PCs is apparent in Fig. 10, where the orbit in (EOF_1^{40}, EOF_2^{40})-space is tilted about the EOF_3^{40} (or EOF_4^{40}) axis when plotted against EOF_3^{40} (or EOF_4^{40}). The projections of these two three-dimensional plots onto the four planes spanned by EOF_1^{40} and EOF_3^{40}, EOF_2^{40} and EOF_4^{40}, EOF_1^{40} and EOF_4^{40}, and EOF_2^{40} and EOF_3^{40} are shown in Fig. 11, where two panels suffice for the four projections. These show the characteristic crossing of orbits near the zero line (Fig. 11a) and maxima near the zero line (Fig. 11b), according to the plane chosen. Further, the nonlinear relationships between the pairs (PC_1^{40}, PC_2^{40}) and (PC_3^{40}, PC_4^{40}) become evident: only when the extrema of PC_1^{40} and PC_2^{40} are weak do PC_3^{40} and PC_4^{40} reach large magnitude (Fig. 11a).

Examination of the time series reveals that these maxima in (PC_3^{40}, PC_4^{40}) occur at times when significant delays occurred in the onset of easterlies in the midstratosphere: particularly the three events in 1964–1965, 1978–1979, and 1988–1989.

b. Long-term variations: EOF_5^{40}

In contrast to the earlier EOFs, which describe propagating, wavelike motions, EOF_5^{40} is a solitary pattern, as for the third pattern with $w = 15$ described in Fraedrich et al. (1993). The three-dimensional phase portrait (Fig. 10) shows that the variations in amplitude of PC_5^{40} lead to a stacking of the orbits of (EOF_1^{40}, EOF_2^{40}); this is due to the long-period variability of PC_5^{40} (Figs. 1 and 2). In Table 3 there is some evidence of correlations between this pattern and the (PC_3^{40}, PC_4^{40})-pair, but stronger anticorrelations with the pair (PC_6^{40}, PC_7^{40}) are evident.

Maximum entropy analysis quantifies the low-frequency variability, showing maximum power at 19, 12, and 7 years; tests have shown no significant linear correlations with the Southern Oscillation index. Note that EOF_5^{40} describes a vertical wind shear, which is presumably related to horizontal temperature gradients by thermal wind balance. Its linear correlation with the solar flux data is about 0.6, which reaches the 99% significance level; in fact, it follows the solar flux for two of the three cycles in the data, but not in the 1970s. Spectral analyses of the solar flux data and EOF_5^{40} do not totally agree with each other. Since there is no clear physical basis for a connection between the solar flux and the tropical zonal wind, these comments must be regarded with caution.

c. The subharmonics: EOF_6^{40} and EOF_7^{40}

From the spectral analysis (Fig. 1b) it is clear that PC_6^{40} and PC_7^{40} have peaks around 14 months. This can also be seen from the EOF patterns (Fig. 7). These represent the subharmonics of the QBO that arise due

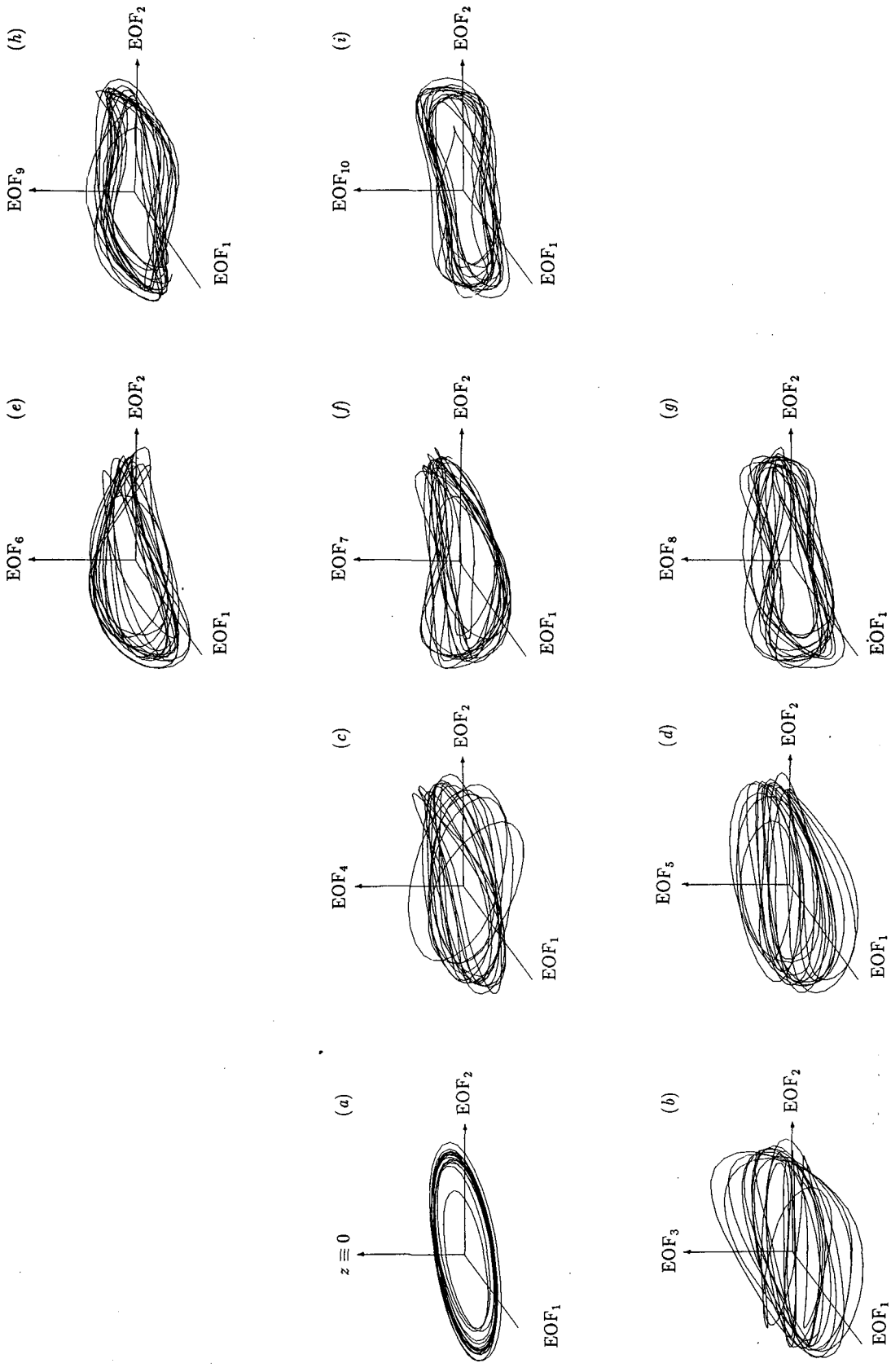

FIG. 10. Phase-space portraits projected onto three-dimensional planes spanned by EOF_1^{40}-EOF_2^{40} and (b)–(i) EOF_3^{40} to EOF_{10}^{40}, respectively. For comparison, (a) gives the two-dimensional plane spanned by the first two EOFs (Fig. 6) displayed in three-dimensional phase space.

TABLE 3. Maxima and minima of the lagged correlation coefficients (top) between the ten leading PCs from EOF analyses of Singapore wind with w = 40 mo and the time delay (in months) of these extrema (bottom). A negative time delay means that the PC in the row leads that in the column by that number of months. The maxima lie above the diagonal and the minima (i.e., strongest anticorrelations) lie on and below the diagonal. On the diagonals there would always be a maximum correlation of 100% at zero lag.

	PC_1	PC_2	PC_3	PC_4	PC_5	PC_6	PC_7	PC_8	PC_9	PC_{10}
PC_1	−94	98	26	16	4	5	8	8	4	6
PC_2	−99	−94	35	27	5	5	8	8	5	7
PC_3	−26	−18	−43	79	48	47	43	22	15	10
PC_4	−33	−27	−85	−53	20	54	50	32	15	22
PC_5	−1	−5	−46	−47	14	55	3	32	5	17
PC_6	−7	−6	−38	−54	−61	−58	64	21	21	4
PC_7	−10	−10	−46	−14	−67	−61	−33	43	30	24
PC_8	−8	−3	−24	−25	−31	−36	−40	−53	68	46
PC_9	−4	−5	−17	−13	−14	−22	−25	−66	−74	61
PC_{10}	−6	−4	−22	−21	−18	−20	−19	−41	−58	−52
	PC_1	PC_2	PC_3	PC_4	PC_5	PC_6	PC_7	PC_8	PC_9	PC_{10}
PC_1	14	7	−16	9	14	−12	−21	21	−21	21
PC_2	7	−14	21	−16	9	21	13	−16	17	−19
PC_3	−15	10	−12	6	−13	7	19	21	−10	21
PC_4	−21	−15	6	11	17	−12	15	18	−15	17
PC_5	−4	21	−13	8	21	19	−15	−21	−18	−10
PC_6	−21	7	17	−12	19	−8	−4	13	−21	17
PC_7	8	13	20	6	−7	−4	7	3	18	21
PC_8	21	−7	8	17	−10	6	3	−6	3	−5
PC_9	−13	18	−10	6	−12	−21	12	3	5	3
PC_{10}	21	7	−13	17	−10	5	19	11	3	5

to its almost-square waveform. Table 3 shows that the cross and autocorrelations between PC_6^{40} and PC_7^{40} maximize at 3–4 and 7 months, respectively, which are one-quarter and one-half of the 14-month periodicity, again indicating a propagating type of oscillation. Their 3D phase portraits (Fig. 10) show relatively little vertical motion in the main parts of the orbits, with slight bending of the (EOF_1^{40}, EOF_2^{40})-orbits at their extrema. Note that these subharmonics should be understood in the local sense (confined to the window) since the pure QBO has a variable period. The time-delayed correlations (Table 3) show some interactions with lower-order patterns over time delays of some months.

d. Shorter periods: EOF_8^{40}-EOF_{10}^{40}

The possibility of an annual modulation of the QBO was discussed by Dunkerton (1990), who showed that the tendency of the easterly phase to stop propagating downward tends to occur in northern winter. The phase–space analysis by Wallace et al. (1993) revealed the tendency of the phase progression of the QBO to discontinue in the same season. In the current analysis there is no hint of an annual synchronization of the four leading EOFs. However, EOF_8^{40} and EOF_9^{40} both have spectral peaks at 12 months (Fig. 1). The auto- and cross-correlations for this EOF pair (Table 3) are not as large as expected for a regularly propagating annual cycle. Phase progression in the (EOF_9^{40}, EOF_8^{40})-plane (Fig. 12) shows the tendency of this EOF pair to lie according to season, with clustering of points in different regions of the phase space. However, the irregular distribution of the seasonal clusters of points show that this is not an exact annual synchronization, in agreement with Dunkerton (1990). The relationship of these two EOFs with the pure QBO signal can be seen from the three-dimensional phase portrait (Fig. 10), where the trajectories are deflected from the EOF_1–EOF_2 plane in preferred seasons and for preferred phases of the QBO. EOF_9^{40} has a secondary spectral peak near 10 months (Fig. 1), the same period as EOF_{10}^{40}, and there is also evidence of some correlation and propagation on the 10-month timescale (Table 3), with the maximum negative autocorrelation of EOF_9^{40} occurring at 5-months delay, rather than at 6 months. Further, there is also a cross correlation between PC_7^{40} and PC_{10}^{40} that maximizes at a time lag of 3 months, also suggesting some propagation through part of the annual cycle. From a statistical point of view there appears to be some of the degeneracy in the EOF analysis. An attempt was made to isolate a 12-month cycle by applying Varimax rotation to the subspace spanned by EOF_6^{40} to EOF_{10}^{40}: this was not successful. This is most likely because such rotation is most effective when the state points in some subspace have a preferred clustering, which is not the case in this analysis where the EOFs are fairly evenly directed in all directions. These results may be best interpreted from a dynamical viewpoint: it seems likely that there is a nonlinear interaction between the forcing of the annual cycle and the basic QBO that precludes their separation in the current analysis.

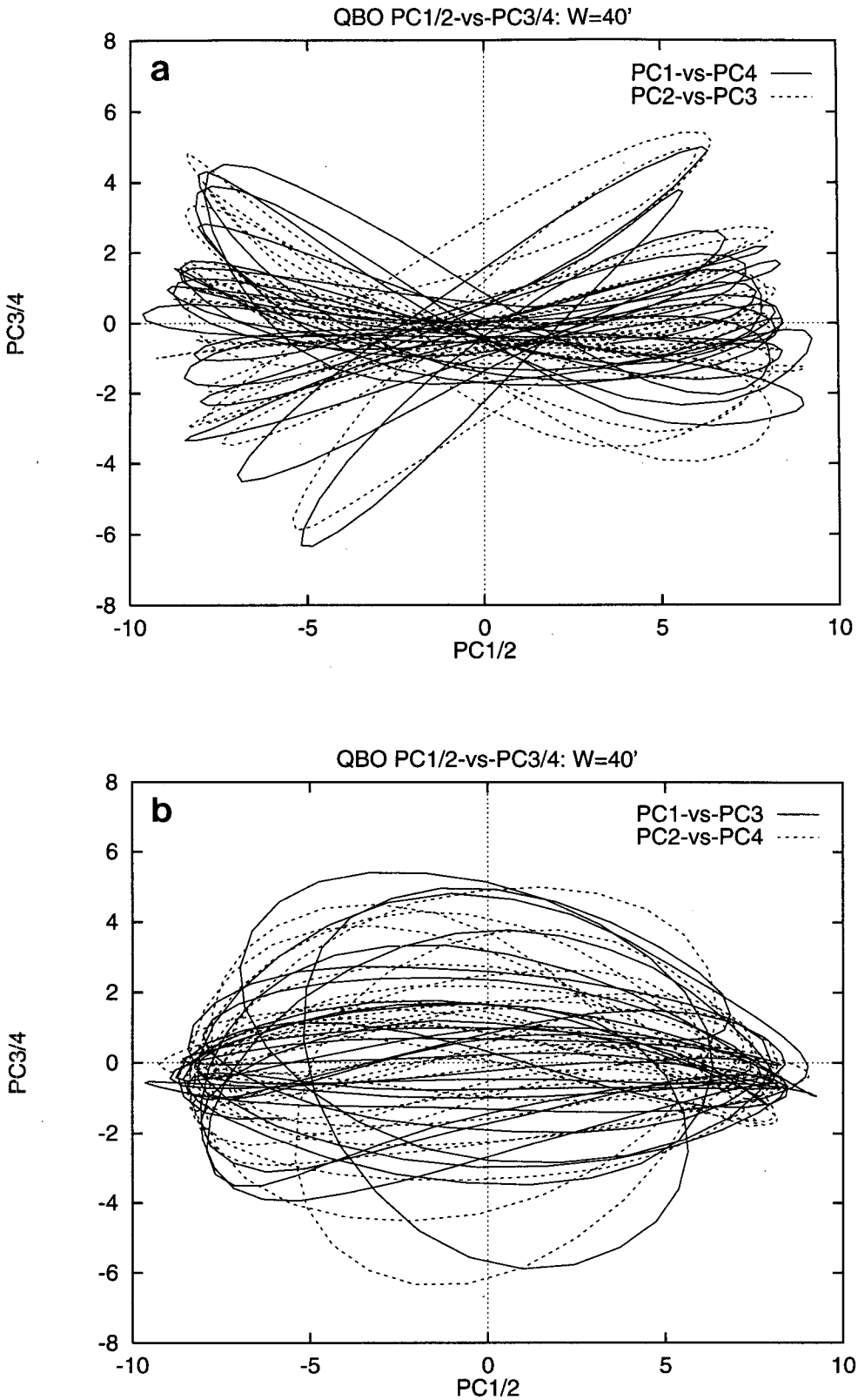

FIG. 11. Two-dimensional phase portraits showing the nonlinear relationships between the pairs of EOFs (EOF_1^{40}, EOF_2^{40}) and (EOF_3^{40}, EOF_4^{40}). The plots show (a) EOF_1^{40} versus EOF_4^{40} and EOF_2^{40} versus EOF_3^{40}. (b) EOF_1^{40} versus EOF_3^{40} and EOF_2^{40} versus EOF_4^{40}.

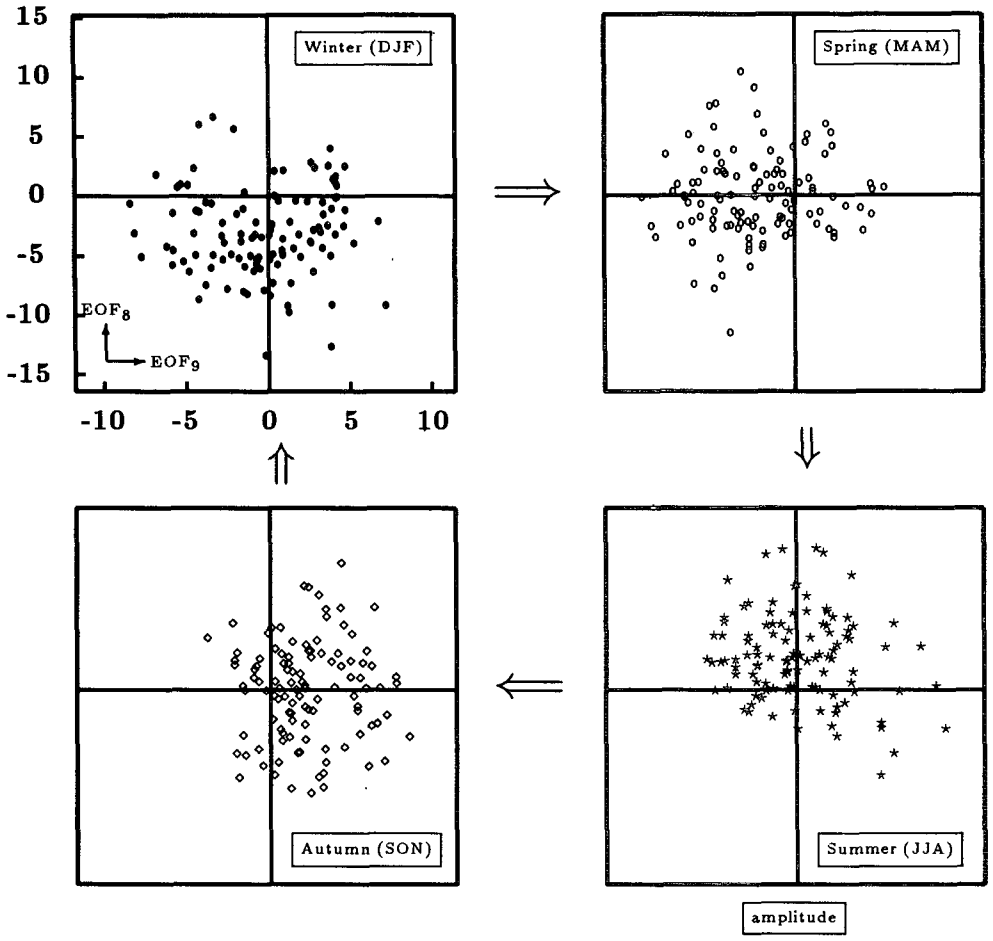

FIG. 12. Scatter diagrams on the (EOF_9^{40}, EOF_8^{40})-plane with the state points separated according to season and marked with different symbols.

6. Conclusions

This study has extended that of Fraedrich et al. (1993) in several ways. The analysis has identified several aspects of the observed QBO, which has a period close to 28 months.

First, the sensitivity of the extended EOF analysis of the tropical wind time series to the choice of window w was examined in some detail. As w is increased, the EOF analysis selectively narrows the signals contained in the first pair of EOFs; their power becomes more concentrated on the QBO period for larger w. For values of w around one-half of the QBO period, the first pair of EOFs represent a QBO signal that displays some stalling of the descent of easterlies. Increasing the window length beyond 28 months results in a smoother oscillation being described by the first pair of EOFs, which is subject to decadal-scale amplitude modulation and some variability in phase propagation. This signal was identified as a "pure QBO," subject to variations in forcing but retaining the character of the Holton–Lindzen (1972) model. This contrasts with the oscillation examined in Fraedrich et al. (1993), where w = 15 was used.

For w = 1, as in Wallace et al. (1993), there is an annual modulation in the phase propagation in the PC_1^1-PC_2^1 plane (as is clear from the power spectrum, Fig. 1), but increasing w leads to the separation of distinct signals for such periods into higher-order EOFs (which are generally degenerate pairs representing propagating waves).

Second, variations in the pure QBO signal were studied. Its period ranges from 22 to 33 months, its mean being close to 28 months. Modulation of the amplitude and phase cannot be simply related to external forcing mechanisms such as ENSO. Its dynamics resemble those of a stochastically driven, characteristic oscillation. With the relatively short time series available, it is not possible to statistically distinguish the pure QBO from a chaotic attractor, but our understanding in terms of the Holton–Lindzen

(1972) model supports the idea of a dynamically driven motion subject to variations, perhaps stochastic, in the forcing mechanisms.

Third, the departures from the QBO were discussed in terms of the higher-order EOFs. These represent departures from the (PC_1^{40}, PC_2^{40})-plane in phase space, allowing for orbit crossings in that plane. The observed QBO is well represented by the pure QBO signal modified by (EOF_3^{40}, EOF_4^{40}), which represent asymmetry in the downward propagation, and (EOF_6^{40}, EOF_7^{40}), which is subharmonic of the QBO, arising because the QBO signal is not a perfect sinusoidal wave. The annual modulation is described by the subspace spanned by (EOF_8, EOF_9). EOF_5 represents the anomaly of the vertical shear of the zonal wind whose time evolution displays a very low frequency change (on the scale of decades). This modulation is very likely related to temperature gradient change in the lower stratosphere; the reason for this change is still unclear to us. There is some evidence of degeneracy of the higher-order EOFs, which may be related to nonlinear interactions between the forcing with annual periodicity and the QBO.

In summary, it seems that the QBO is subject to both deterministic and stochastic forcing mechanisms. The deterministic factors are suggested by the existence of a characteristic mode driven by wave-mean flow interaction, resulting in a smooth and regular trajectory. There is evidence of annual modulation, but the annual cycle and the QBO seem to interact in a nonlinear manner. Long-term variations in the pure QBO are likely to be caused by stochastic variations in the tropical wave amplitudes in the Holton–Lindzen (1972) model.

Studies such as this can isolate statistical properties of basic dynamical features of the atmosphere. However, since the forcing mechanisms are not taken into account, the causality cannot be isolated. There are clearly signals due to the annual cycle in the analysis, which can be explained by annual variations in the forcing due to tropical waves (Maruyama 1991; Dunkerton 1990) or the vertical advection (Dunkerton 1991; Pawson et al. 1993a). However, forcing anomalies due to, say, ENSO cannot be isolated. Possible future studies must therefore include more information about the forcing mechanisms in the statistical analysis. The value of modelling studies in isolating causality cannot be underestimated.

Acknowledgments. We are grateful to Barabara Naujokat for providing the tropical wind data used in this study. Most of this research was performed by R.-S. W. for his Ph.D. thesis at the FU Berlin, supported by the German Ministry for Research and Technology (BMFT), Grant 07KFT306. SP's research was partially supported by the BMFT, Grant 01OFP9207. Constructive comments by Dr. T. J. Dunkerton, two further referees, and the editor Dr. M. LeMone led to substantial improvements in this study.

REFERENCES

Box, G. E. P., and G. M. Jenkins, 1976: *Time Series Analysis, Forecasting and Control.* rev. ed., Holden-Day, 575 pp.

Dunkerton, T. J., 1990: Annual variation of deseasonalized mean flow acceleration in the equatorial lower stratosphere. *J. Meteor. Soc. Japan,* **68,** 499–508.

——, 1991: Nonlinear propagation of zonal winds in an atmosphere with Newtonian cooling and equatorial wavedriving. *J. Atmos. Sci.,* **48,** 236–263.

Fraedrich, K., S. Pawson, and R. Wang, 1993: An EOF analysis of the vertical-time delay structure of the Quasi-Biennial Oscillation. *J. Atmos. Sci.,* **50,** 3357–3365.

Hamilton, K., 1981: The vertical structure of the QBO: Observations and theory. *Atmos.-Ocean,* **19,** 236–250.

Hirota, I., and Y. Sato, 1969: Periodic variation of the winter stratospheric circulation and intermittent vertical propagation of planetary waves. *J. Meteor. Soc. Japan,* **47,** 390–402.

Holton, J. R., and R. S. Lindzen, 1972: An updated theory for the Quasi-Biennial Oscillation of the tropical stratosphere. *J. Atmos. Sci.,* **29,** 1076–1080.

Lindzen, R. S., and C.-Y. Tsay, 1975: Wave structure of the tropical stratosphere over the Marshall Islands area during 1 April–1 July 1958. *J. Atmos. Sci.,* **32,** 2008–2021.

Lorenz, E. N., 1963: Deterministic nonperiodic flow. *J. Atmos. Sci.,* **20,** 130–141.

Maruyama, T., 1991: Annual and QBO-synchronized variations of lower-stratospheric equatorial wave activity over Singapore during 1961–1989. *J. Meteor. Soc. Japan,* **69,** 219–232.

——, and Y. Tsuneoka, 1988: Anomalously short duration of the easterly wind phase of the QBO at 50 hPa in 1987 and its relationship to an El Niño event. *J. Meteor. Soc. Japan,* **66,** 629–633.

Naujokat, B., 1986: An update of the observed Quasi-Biennial Oscillation of the stratospheric winds over the tropics. *J. Atmos. Sci.,* **43,** 1873–1877.

Pawson, S., K. Labitzke, B. Naujokat, R.-S. Wang, and K. Fraedrich, 1993a: Inter-seasonal tropical–extra-tropical interactions observed in the stratosphere. *Coupling Processes in the Lower and Middle Atmosphere,* NATO ASI Series, E. V. Thrane, T. A. Blix, and D. C. Fritts, Eds., Kluwer Academic Publishers, 35–47.

——, ——, R. Lenschow, B. Naujokat, B. Rajewski, M. Wiesner, and R.-C. Wohlfahrt, 1993b: Climatology of the Northern Hemisphere Stratosphere Derived from Berlin Analyses. Part I: Monthly Means. *Meteorologische Abhandlungen (Neue Folge),* **A7**(3), Verlag von Dietrich Reimer, 299 pp.

Plumb, R. A., 1977: The interaction of two internal waves with the mean flow: Implications for the theory of the Quasi-Biennial Oscillation. *J. Atmos. Sci.,* **34,** 1847–1858.

——, and R. C. Bell, 1982: A model of the Quasi-Biennial Oscillation on an equatorial beta plane. *Quart. J. Roy. Meteor. Soc.,* **108,** 335–352.

Schuster, H. G., 1989: *Deterministic Chaos.* VCH Verlagsgesellschaft, 270 pp.

Takahashi, M., and J. R. Holton, 1991: The mean zonal flow response to Rossby wave and gravity wave forcing in the equatorial lower stratosphere: Relationship to the QBO. *J. Atmos. Sci.,* **48,** 2078–2087.

Wallace, J. M., 1973: General circulation of the tropical lower stratosphere. *Rev. Geophys. Space Phys.,* **11,** 191–222.

——, L. Panetta, and J. Estberg, 1993: A phase–space representation of the equatorial stratospheric Quasi-Biennial Oscillation. *J. Atmos. Sci.,* **50,** 1751–1762.

Wang, R.-S., 1994: *A Phase-Space Approach to Atmospheric Dynamics Based on Observational Data—Theory and Applications. Meteor. Abhandl. (Neue Folge),* **A8**(2), Verlag von Dietrich Reimer, 227 pp.

Weare, B. C., and J. S. Nasstrom, 1982: Examples of extended empirical orthogonal function analysis. *Mon. Wea. Rev.,* **110,** 481–485.

Xu, J.-S., 1992: On the relationship between the stratospheric Quasi-Biennial Oscillation and the tropospheric Southern Oscillation. *J. Atmos. Sci.,* **49,** 725–734.

Yoden, S., and J. R. Holton, 1988: A new look at equatorial Quasi-Biennial Oscillation models. *J. Atmos. Sci.,* **45,** 2703–2717.